

Nature-Guided Cognitive Evolution for Predicting Dissolved Oxygen Concentrations in North Temperate Lakes

Runlong Yu¹, Robert Ladwig², Xiang Xu³, Peijun Zhu⁴,

Paul C. Hanson⁵, Yiqun Xie⁶, Xiaowei Jia¹

¹University of Pittsburgh, ²Aarhus University, ³University of Science and Technology of China

⁴Georgia Institute of Technology, ⁵University of Wisconsin-Madison, ⁶University of Maryland-College Park
{ruiy59,xiaowei}@pitt.edu,rladwig@ecos.au.dk,demon@mail.usstc.edu.cn,zpj@gatech.edu,pchanson@wisc.edu,xie@umd.edu

ABSTRACT

Predicting dissolved oxygen (DO) concentrations in north temperate lakes requires a comprehensive study of phenological patterns across various ecosystems, which highlights the significance of selecting phenological features and feature interactions. Process-based models are limited by partial process knowledge or oversimplified feature representations, while machine learning models face challenges in efficiently selecting relevant feature interactions for different lake types and tasks, especially under the infrequent nature of DO data collection. In this paper, we propose a *Nature-Guided Cognitive Evolution (NGCE)* strategy, which represents a multi-level fusion of adaptive learning with natural processes. Specifically, we utilize metabolic process-based models to generate simulated DO labels. Using these simulated labels, we implement a multi-population cognitive evolutionary search, where models, mirroring natural organisms, adaptively evolve to select relevant feature interactions within populations for different lake types and tasks. These models are not only capable of undergoing crossover and mutation mechanisms within intra-populations but also, albeit infrequently, engage in inter-population crossover. The second stage involves refining these models by retraining them with real observed labels. We have tested the performance of our NGCE strategy in predicting daily DO concentrations across a wide range of lakes in the Midwest, USA. These lakes, varying in size, depth, and trophic status, represent a broad spectrum of north temperate lakes. Our findings demonstrate that NGCE not only produces accurate predictions with few observed labels but also, through gene maps of models, reveals sophisticated phenological patterns of different lakes.

1 INTRODUCTION

The concentration of dissolved oxygen (DO) in lakes, as the indicator of water quality and ecosystem health, plays a key role in sustaining aquatic biodiversity and ensuring water safety for human consumption [60]. DO concentrations are shaped not just by the exchange of oxygen between air and water, but also by the metabolic processes of primary production and respiration [50]. As articulated by Edward A. Birge one century ago [4]: The fluctuations in a lake's oxygen illustrate its "life cycle" more clearly than many other ecological indicators. This is particularly evident in nutrient-rich eutrophic lakes, where algal blooms can significantly deplete oxygen, creating detrimental "dead zones" for aquatic life.

DO concentration is closely intertwined with ecosystem phenology, influenced by morphometric and geographic information, mass fluxes, weather conditions, trophic state, and watershed land use. In deeper lakes, for instance, increased light limitation and decreased mixing with the oxygen-rich surface layers often result

in diminished oxygen in deeper areas [42, 49]. Temperature fluctuations also play a pivotal role in oxygen solubility and biochemical activities [53]. Land use changes can reshape DO patterns and metabolism phenology [22, 61]. Accurate prediction of DO concentrations requires a comprehensive study of these phenological patterns across various ecosystems, which entails utilizing long-term data encompassing a wide range of features. This highlights the significance of selecting phenological features and feature interactions, which offers a basis for analyzing the dynamics of the metabolism of lakes and their evolution in response to external factors, as well as internal physical-chemical-biological interactions.

Given the importance of DO concentration prediction, scientists from multiple domains, including limnology, hydrology, meteorology, and environmental engineering, have developed physically and ecologically simplified process-based models to simulate different components of aquatic ecosystem states and processes. Numerous aquatic ecosystem models (AEMs) are designed to assess the impact of both external and internal factors on ecosystems, often combining hydrodynamic and water quality models with interconnected feedback loops [20]. Notable examples include hydrodynamic models like DYRESM [13], GLM [17], MyLake [48]. More advanced vertical one-dimensional AEMs include GLM-AED [17], WET [41], and PCLake [21]. However, these models, despite being grounded in physical principles like mass and energy conservation, are approximations due to partial process knowledge. Their accuracy and reliability are often constrained by either limited understanding or oversimplified feature representations.

Advanced data-driven approaches like deep learning [30], known for their success in vision and language processing, are considered alternatives to process-based models for predicting DO concentrations. However, applying these methods involves distinct challenges. Firstly, predicting DO concentrations involves sophisticated phenological patterns in various ecosystems, which requires analyzing a wide array of features. Equally enumerating all feature interactions can bring unnecessary noise and complicate the training process. Meanwhile, manually selecting relevant interactions requires substantial manual labor and may also miss crucial subtleties due to limited knowledge about complex ecosystems. Secondly, most approaches rely on global models built under expert guidance and lack the flexibility to adapt to various tasks and datasets. As a result, they often fail to select relevant feature interactions for different lake types and tasks and thus cannot guarantee effective model learning across different scenarios. Finally, the observations of DO concentration are often very sparse, primarily due to the high material costs needed for data collection. Such sparse DO labels pose a significant challenge for training reliable and accurate models.

To address these challenges, we propose a *Nature-Guided Cognitive Evolution (NGCE)* strategy, motivated by a multi-level fusion of adaptive learning with natural processes. NGCE generates simulated labels using a metabolic process-based model to address sparsely observed DO concentration. To analyze sophisticated phenological patterns, we implement an evolutionary learning algorithm to select feature interactions, simulating the natural adaptability of organisms to their environment. It uses multi-population models to cater to various lake types and tasks, reflecting how species thrive in diverse habitats. Finally, NGCE enhances model accuracy by retraining with observed DO concentration data.

Specifically, We simplify our analysis by dividing the water column into two distinct layers with separate oxygen and metabolic kinetics: the epilimnion (upper surface layer) and the hypolimnion (lower bottom layer), treating their DO dynamics as two tasks. We separately simulate their DO concentrations by modeling vertical transport processes and metabolic reactions. Then, we propose a multi-population cognitive evolutionary search, where we conceptualize interactions as genomes, models as organisms within a population, and tasks as natural environments. These models are not only capable of undergoing crossover and mutation mechanisms within intra-populations but also, albeit infrequently, engage in inter-population crossover. This enables our models to dynamically select time-varying phenological features and their interactions for predicting simulated DO labels across different lake types and tasks. The final stage of our approach refines these evolved models using real-world observed DO concentration data. This mirrors natural genetic decoding, where selected features and interactions are further optimized to reflect actual ecological dynamics. We have tested the effectiveness of our NGCE strategy using data from 375 lakes in the Midwest, USA, covering 41 years, representing a diverse sample of north temperate lakes. The main contributions of this paper can be highlighted as follows:

- We propose the NGCE strategy as a multi-level fusion of adaptive learning with natural processes. It leverages a process-based model to generate simulated labels for feature interaction selection and further refines the model using observed labels, effectively addressing the scarcity of DO concentration labels.
- We propose a multi-population cognitive evolutionary search, inspired by the natural selection, to emulate the adaptability of natural organisms. This leads to the populations of models specifically designed for different lake types and predictive tasks, resulting in adaptive models for diverse lake environments.
- We validate the effectiveness of our NGCE strategy applying it to predict daily DO concentrations in diverse north temperate lakes in the Midwest, USA. The results demonstrate that NGCE not only achieves accurate predictions with few observed labels but also reveals sophisticated phenological patterns of different lakes.

2 PRELIMINARY

2.1 Problem Formulation

Our goal is to predict the DO concentration at a daily scale. We have access to phenological features \mathbf{x}_t for each lake on date t , and on certain days, we record DO concentrations y_t in both the epilimnion y_t^{epi} and hypolimnion y_t^{hyp} layers. These features, spanning m diverse fields $\mathbf{x}_t = \{x_t^1, \dots, x_t^m\}$, encompass morphometric and

geographic details such as lake area, depth, and shape; flux-related data like ecosystem and sedimentation fluxes; weather factors comprising wind speed and temperature; a range of trophic states from dystrophic to eutrophic; and diverse land use proportions extending from forests to wetlands. To process these features, we use an embedding layer to convert them into a series of multi-field feature embeddings $\mathbf{f}_t = [\mathbf{f}_t^1, \dots, \mathbf{f}_t^m]$, where $\mathbf{f}_t^i = \text{embed}(x_t^i)$. Our model uses these embeddings to predict DO concentrations \hat{y}_t for both the epilimnion \hat{y}_t^{epi} and hypolimnion \hat{y}_t^{hyp} .

2.2 Metabolic Process-based Model

We introduce a metabolic process-based model to generate simulated labels [29]. Our study focuses on changes in ecosystem-scale metabolic fluxes in lakes that stratify (a vertical density difference over 0.05 kg/m^3 between surface and bottom layers, and the presence of a thermocline). These lakes largely adhere to the vertical one-dimensional model assumption [17, 21, 41], which posits a more pronounced density gradient vertically than horizontally. During stratification, we simplify the water column into two mixed volumes: the upper epilimnion and the lower hypolimnion, treating the thermocline depth as a dividing barrier between both volumes. Our model primarily focuses on metabolic dynamics during warmer periods, excluding inverse stratification periods in ice-covered winters. This is due to the scarce availability of under-ice DO data and the heightened significance of abiotic-biotic interactions in warmer conditions. For simplicity, we represent the direct flux features that either augment or diminish DO concentrations as F within our metabolic process-based model. Upon obtaining observed DO data, we generate posterior estimates for the process-based model to ascertain F effectively [29].

We integrate information from a hydrodynamic lake model into a metabolism model to study each lake. By constructing a time series of temperatures and volumes for both the epilimnion and hypolimnion, these features are utilized in our process-based metabolism model to simulate DO concentrations and their respective fluxes. Our model simplifies the ordinary differential DO equation for each layer into a discrete, first-order linear solution using an explicit forward Euler scheme with a daily timestep. During stratified conditions, we calculate the DO concentrations over time in the epilimnion as: $\tilde{y}_{t+1}^{epi} = \left(\tilde{y}_t^{epi} + \left(F_t^{ATM} + F_t^{NEP,epi} \pm F_t^{ENT,epi} \pm F_t^{DIF,epi} \right) \times \Delta t \right) \times \frac{V_t^{epi}}{V_{t+1}^{epi}}$, where \tilde{y}_t^{epi} denotes the simulated DO concentration in the epilimnion at time t , as estimated by this metabolic process-based model, V_t^{epi} indicates the volume of this epilimnion at time t , F represents the flux features: In the epilimnion it comprises atmospheric exchange (F^{ATM}), net ecosystem production in the epilimnion ($F^{NEP,epi}$), DO entrainment from or into the hypolimnion by turbulent flow ($F^{ENT,epi}$), and the diffusive DO flux between layers ($F^{DIF,epi}$).

The same metabolic process applies to the hypolimnion, where the flux features F to DO concentrations over time in the hypolimnion are net ecosystem production ($F^{NEP,hyp}$), mineralization through sediment oxygen demand (F^{SED}), DO entrainment into or from the epilimnion by turbulent flow ($F^{ENT,hyp}$), and the diffusive DO flux between layers ($F^{DIF,hyp}$): $\tilde{y}_{t+1}^{hyp} = \left(\tilde{y}_t^{hyp} + \left(F_t^{NEP,hyp} - \right.$

$F_t^{SED} \pm F_t^{ENT, hyp} \pm F_t^{DIF, hyp} \times \Delta t \times \frac{V_t^{hyp}}{V_{t+1}^{hyp}}$, where \tilde{y}_t^{hyp} denotes the simulated DO concentration in the hypolimnion for lake l at time t , V_t^{hyp} indicates the volume of the hypolimnion at time t .

3 NATURE-GUIDED COGNITIVE EVOLUTION

In this section, we will introduce the proposed *Nature-Guided Cognitive Evolution (NGCE)* strategy, which consists of two stages of learning, i.e., feature selection stage, and model functioning stage. The overall framework is illustrated in Figure 1. The strategy begins with the feature selection stage, where simulated labels are leveraged to facilitate a multi-population cognitive evolutionary search for identifying relevant features and interactions. Following this, the model functioning stage applies these selected features and interactions for further refinement with real observed labels.

3.1 Feature Selection Stage

In this subsection, we detail the feature selection stage, employing simulated labels \tilde{y}_t to train a multi-population cognitive evolutionary search algorithm. We begin by introducing the establishment of multiple populations, followed by an explanation of how each individual within these populations is modeled. Subsequently, we delve into the fundamental mutation and crossover mechanisms. Lastly, we provide an instantiation of the algorithm.

3.1.1 Identifying different lake types. We first categorize lakes into different types using lake characteristics that have a direct impact on oxygen dynamics. In particular, we consider the characteristics of surface area and volume because lakes with expansive surface areas facilitate more effective oxygen exchange with the atmosphere, while those with larger volumes are prone to higher oxygen consumption in deeper waters during summer, owing to limited oxygen replenishment from the surface. To categorize the diverse array of lakes in our dataset \mathcal{L} , we use a balanced K-means clustering algorithm to create lake clusters of more uniform sizes [38], which ensures a more equitable distribution of lake types in our analysis. By applying balanced K-means clustering, we group lakes into four distinct categories based on their volume and area: small lakes \mathcal{L}_S , medium lakes \mathcal{L}_M , large lakes \mathcal{L}_L , and extra-large lakes \mathcal{L}_{XL} .

3.1.2 Multi-population of feature interaction selection models. The use of population in evolutionary learning has been proven to make search processes less prone to settle in local optima [16, 39, 56]. In our strategy, each population is a set of models specifically designed for distinct lake types and tasks. Consequently, we have established eight unique populations: \mathcal{P}_S^{epi} , \mathcal{P}_S^{hyp} , \mathcal{P}_M^{epi} , \mathcal{P}_M^{hyp} , \mathcal{P}_L^{epi} , \mathcal{P}_L^{hyp} , \mathcal{P}_{XL}^{epi} , \mathcal{P}_{XL}^{hyp} . For example, models within \mathcal{P}_S^{epi} are trained using data from small lakes \mathcal{L}_S and simulated labels for these lakes in the epilimnion \tilde{y}^{epi} .

In our population-based search with a size of n (where $n > 1$), we initialize each population with n models for feature interaction selection: $\mathcal{P} = \{\mathcal{M}_1, \dots, \mathcal{M}_n\}$. We liken each feature interaction selection model to a natural organism evolving to optimize its traits for greater fitness. These traits, inherited via an organism's genomes, are derived from the relationship between features and operations, analogous to nucleotides and their linkages. Following various linkages of nucleotides, we enrich our operation set by introducing four types of operations $\mathbf{g} = \{\oplus, \otimes, \boxplus, \boxtimes\}$, which are

highly used in previous work [26, 32, 51, 64]. Specifically, these operations include element-wise sum (\oplus), element-wise product (\otimes), concatenation with a feed-forward layer (\boxplus), and element-wise product with a feed-forward layer (\boxtimes). In our feature interaction selection model, if g_k is a chosen operation from \mathbf{g} , an interaction $g_k(\mathbf{f}_t^i, \mathbf{f}_t^j)$ is defined by applying the operation g_k to a pair of features $(\mathbf{f}_t^i, \mathbf{f}_t^j)$.

Our strategy is designed to enhance model fitness by favoring the preservation of beneficial genetic information, motivating us to discern and prioritize important features and their interactions through a set of relevance parameters, thereby strengthening those that are relevant while diminishing or mutating less contributory ones. In this context, we define relevance parameters for features \mathbf{f}_t and interactions $\tilde{g}(\mathbf{f}_t)$ as $\boldsymbol{\alpha} = \{\alpha_i | 1 \leq i \leq m\}$ and $\boldsymbol{\beta} = \{\beta_{i,j} | 1 \leq i < j \leq m\}$, respectively. Here, $\tilde{g}(\mathbf{f}_t)$ denotes the application of any operations from \mathbf{g} to each pair of features. The predictive response of our model at specific time steps is formulated as:

$$\tilde{y}_t = \mathcal{M}(\boldsymbol{\alpha} \cdot \mathbf{f}_t, \boldsymbol{\beta} \cdot \tilde{g}(\mathbf{f}_t)). \quad (1)$$

where \mathcal{M} can be any individual model in the population. We use a sequence encoder with a Long-Short Term Memory (LSTM) network [18] to efficiently encode temporal information and feature interaction dynamics. The model \mathcal{M} is thus depicted as:

$$\begin{aligned} \mathbf{h}_t' &= \text{LSTM}([\boldsymbol{\alpha} \cdot \mathbf{f}_t, \boldsymbol{\beta} \cdot \tilde{g}(\mathbf{f}_t)]; \mathbf{h}_{t-1}'), \\ \hat{y}_t &= \mathbf{W}' \cdot \mathbf{h}_t' + \mathbf{b}', \end{aligned} \quad (2)$$

where \mathbf{h}_t' represents a series of hidden states, and \mathbf{W}' and \mathbf{b}' denote the weight and bias parameters, respectively. The loss function for model \mathcal{M} , calculated using simulated labels \tilde{y}_t , is defined as:

$$\mathcal{L}(\mathcal{M}) = \frac{1}{|B|} \sum_{(l,t) \in B} (\tilde{y}_t - \hat{y}_t)^2, \quad (3)$$

where B denotes the set of instance indices within a mini-batch.

We use a regularized dual averaging (RDA) optimizer to differentiate between relevant and irrelevant feature interactions, learning the relevance parameters $\boldsymbol{\alpha}$ and $\boldsymbol{\beta}$ through this process [6, 62]. When the absolute value of the cumulative gradient average value in a certain position in $\boldsymbol{\alpha}$ or $\boldsymbol{\beta}$ is less than a threshold, the weight of that position in relevance parameters will be set to 0, resulting in the sparsity of the relevance [33, 62]. Meanwhile, feature embeddings are optimized using the Adam optimizer [27]. Unlike AutoML [34], which categorizes $\boldsymbol{\alpha}$ and $\boldsymbol{\beta}$ as high-level decisions and treats feature embeddings as lower-level variables for bi-level optimization, our approach simplifies this process. AutoML operates under the premise that accurate operation selection is contingent upon the effective learning of feature embeddings, thereby enabling $\boldsymbol{\alpha}$ and $\boldsymbol{\beta}$ to "make their proper decision." To circumvent the complex and costly inner optimization of gradients for feature embeddings and relevance parameters $\boldsymbol{\alpha}$, $\boldsymbol{\beta}$, we update them jointly using one-level optimization with gradient descent on the training set, given as:

$$\begin{aligned} &\nabla_{\mathbf{f}} \mathcal{L}(\mathbf{f}_{iter-1}, \boldsymbol{\alpha}_{iter-1}, \boldsymbol{\beta}_{iter-1}) \\ &\text{and } \nabla_{\boldsymbol{\alpha}, \boldsymbol{\beta}} \mathcal{L}(\mathbf{f}_{iter-1}, \boldsymbol{\alpha}_{iter-1}, \boldsymbol{\beta}_{iter-1}). \end{aligned} \quad (4)$$

3.1.3 Mutation mechanism and crossover mechanism. With our definitions of population and feature interaction selection models, we further detail both the mutation and crossover mechanisms in

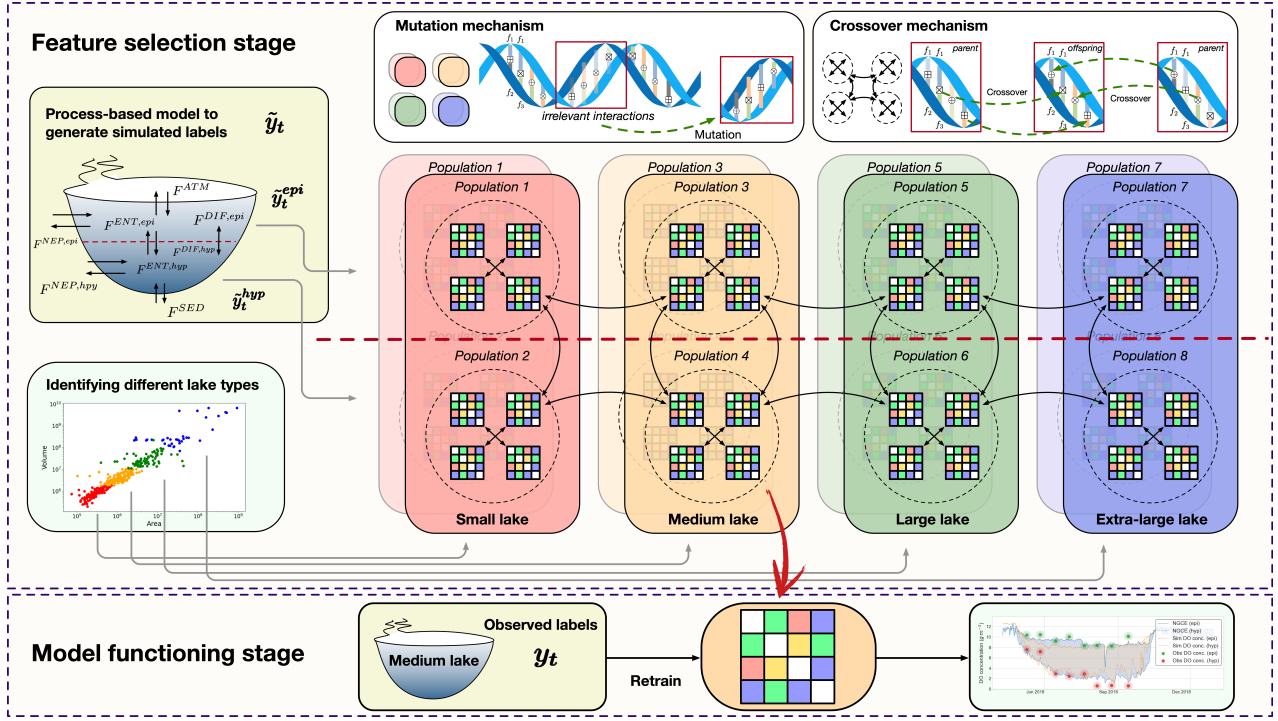


Figure 1: An illustration of the NGCE strategy. Feature selection stage: Leveraging a metabolic process-based model to generate simulated labels for a multi-population cognitive evolutionary search, aimed at selecting relevant features and interactions. Model functioning stage: Employing these selected features and interactions for further refinement with real observed labels.

our strategy. Notably, the crossover mechanism is bifurcated into intra-population and inter-population crossover.

Mutation mechanism. The mutation serves as a fundamental mechanism of our search process, primarily aiming at discriminating relevant and irrelevant feature interactions in the current model (the parent), then mutates the operations associated with irrelevant interactions into alternative operations, thus generating a new model (the offspring). Specifically, for an interaction $g_k(f_i^i, f_i^j)$, mutation is triggered with a probability σ after every τ steps if the relevance parameter $\beta_{i,j}$ drops below a threshold λ . In other words, to regenerate a new interaction, the operation g_k of the interaction $g_k(f_i^i, f_i^j)$ mutates into another operation g_l , given as:

$$g_k = \begin{cases} g_l & \text{with probability } \sigma, & \text{if } \beta_{i,j} < \lambda, \\ g_k, & & \text{otherwise.} \end{cases} \quad (5)$$

where g_l is randomly selected from the operation set as $g_l = \{g \mid g \in \mathcal{G}, g \neq g_k\}$. The new interaction $g_l(f_i, f_j)$ replaces the irrelevant interaction $g_k(f_i, f_j)$, and its corresponding relevance $\beta_{i,j}$ is reset. Consequently, the parent model \mathcal{M} evolves into its offspring \mathcal{M}' , which incorporates these fresh interactions with revised relevance β' , and maintains features with relevance α' inherited from α .

Intra-population crossover mechanism. Given a population $\mathcal{P} = \{\mathcal{M}_1, \dots, \mathcal{M}_v, \dots, \mathcal{M}_n\}$, we use $\beta^{\mathcal{M}_v}$ to denote the relevance parameters of interactions for each model \mathcal{M}_v . The obtained $\beta^{\mathcal{M}_v}$ can vary across different models in \mathcal{P} . Therefore, within this population, the models may have a variety of operations for interacting with each feature pair (f_i, f_j) , represented as $g_{i,j}^{\mathcal{P}} =$

$\{g_{i,j}^{\mathcal{M}_1}, \dots, g_{i,j}^{\mathcal{M}_v}, \dots, g_{i,j}^{\mathcal{M}_n}\}$. The intra-population crossover mechanism aims to select the most suitable operation (of which interaction has the largest relevance) within the population to apply on the feature pair for the offspring model \mathcal{M}' , given as:

$$g_{i,j}^{\mathcal{M}'} = \arg \max_{g_{i,j}^{\mathcal{P}}} \beta_{i,j}^{\mathcal{M}_v}. \quad (6)$$

Meanwhile, the relevance parameters of interactions in this offspring model are inherited from their respective parent models (i.e., the selected \mathcal{M}_v).

Inter-population crossover mechanism. In two distinct populations $\mathcal{P}_A = \{\mathcal{M}_1^A, \dots, \mathcal{M}_v^A, \dots, \mathcal{M}_n^A\}$ and $\mathcal{P}_B = \{\mathcal{M}_1^B, \dots, \mathcal{M}_v^B, \dots, \mathcal{M}_n^B\}$, where $\beta^{\mathcal{M}_v^A}$ and $\beta^{\mathcal{M}_v^B}$ denote the relevance of interactions for two populations, respectively. The inter-population crossover mechanism works as follows: For each feature pair (f_i, f_j) , we select the most suitable operation from \mathcal{P}_B to interact on the feature pair in the offspring model of \mathcal{P}_A . Conversely, the most suitable operation of the feature pair from \mathcal{P}_A is selected for the offspring model of \mathcal{P}_B , given as:

$$g_{i,j}^{\mathcal{M}_v^A} = \arg \max_{g_{i,j}^{\mathcal{P}_B}} \beta_{i,j}^{\mathcal{M}_v^B}, \quad g_{i,j}^{\mathcal{M}_v^B} = \arg \max_{g_{i,j}^{\mathcal{P}_A}} \beta_{i,j}^{\mathcal{M}_v^A}. \quad (7)$$

Meanwhile, the relevance parameters of interactions in the offspring models are inherited from their respective parent models.

3.1.4 Instantiation of the search process. Leveraging the mutation mechanism and both intra- and inter-population crossover mechanisms, we introduce an implementation of the multi-population cognitive evolutionary search, as outlined in Algorithm 1. Initially,

the algorithm randomly initializes eight distinct model populations (line 1). It proceeds with a series of iterative steps (lines 6-27), continuing until convergence. Each iteration involves optimizing offspring models and their relevance parameters within each population.

For every τ iterations, the algorithm (lines 10-14) selects and replaces the worst model \mathcal{M} in each population \mathcal{P} based on the designated loss function, referred to Eq. (3), given as:

$$\mathcal{M} = \arg \max_{\mathcal{M}_v \in \mathcal{P}} L(\mathcal{M}_v). \quad (8)$$

When the algorithm replaces the worst model \mathcal{M} with the offspring model \mathcal{M}' , a new offspring \mathcal{M}' is generated through intra-population crossover and subsequent mutation, enhancing genotypic diversity, thus enabling the search process to effectively avoid local optima and explore global regions.

For every $ep \times \tau$ iterations (lines 18-25), a pair of populations $\mathcal{P}_A, \mathcal{P}_B$ are randomly selected based either on a shared task (i.e., epilimnion or hypolimnion) across different lake types or on the same lake type but with different tasks. This leads to the generation of new offspring models $\mathcal{M}'_A, \mathcal{M}'_B$ via inter-population crossover between $\mathcal{P}_A, \mathcal{P}_B$, promoting the transfer of advantageous genotypic patterns across different lake types and tasks. Simultaneously, each remaining population generates its offspring \mathcal{M}' through intra-population crossover, followed by the mutation of all offspring.

Finally, the algorithm culminates by delivering a set of the best models, one from each population (line 28), thereby ensuring a comprehensive exploration and exploitation of the search space across diverse environmental contexts.

3.2 Model Functioning Stage

Drawing inspiration from nature's replication and transcription processes, which translate genetic information into protein sequences to equip organisms with diverse functions, we proceed to a model functioning stage. Here our objective is to refine the model by leveraging selected features and interactions. At this stage, we select the corresponding model by the lake type and task, and use observed labels for the model refinement. Relevant features and interactions are selected according to their relevance parameters α, β . If $\alpha_i = 0$ or $\beta_{i,j} = 0$, the corresponding features or interactions are fixed to be discarded permanently. Given the scarcity of observed data, we inherit parameters from the preceding LSTM to ensure the model's effective learning, given as:

$$\begin{aligned} \mathbf{h}_t^o &= \text{LSTM}([\alpha \cdot \mathbf{f}_t, \beta \cdot \mathbf{g}(\mathbf{f}_t)]; \mathbf{h}_{t-1}^o) \\ \hat{y}_t &= \mathbf{W}^o \cdot \mathbf{h}_t^o + \mathbf{b}^o \end{aligned} \quad (9)$$

where \mathbf{h}_t^o represents a series of hidden states, with \mathbf{W}^o and \mathbf{b}^o as the weight and bias parameters, respectively. The relevance α, β are fixed and serve as attention units.

To bridge the gap between abundant simulated and scarce observed labels, we crafting a masked LSTM by blending sparse observations with simulated labels through weighted imputation and gradient adjustments. This helps mitigates the scarcity in observed labels. This leads to a loss function combining both observed and simulated data, as follows:

$$L(\mathcal{M}) = \frac{1}{|B|} \sum_{(l,t) \in B} \mathbb{I}(y_t) (y_t - \hat{y}_t)^2 + \rho (1 - \mathbb{I}(y_t)) (\tilde{y}_t - \hat{y}_t)^2, \quad (10)$$

Algorithm 1 Multi-population Cognitive Evolutionary Search

Input: Training dataset of four types of lakes $\mathcal{L}_S, \mathcal{L}_M, \mathcal{L}_L, \mathcal{L}_{xL}$, each lake l has features \mathbf{f}_t , simulated DO labels $\tilde{y}_t^{epi}, \tilde{y}_t^{hyp}$ over T days; operation set \mathbf{g} .

```

1: Initialize eight populations  $\mathcal{P}_S^{epi}, \mathcal{P}_S^{hyp}, \mathcal{P}_M^{epi}, \mathcal{P}_M^{hyp}, \mathcal{P}_L^{epi},$ 
    $\mathcal{P}_L^{hyp}, \mathcal{P}_{xL}^{epi}, \mathcal{P}_{xL}^{hyp}$ , of which any  $\mathcal{M}$  has initialized  $\alpha$  and  $\beta$ .
2: for each  $\mathcal{P}$  do
3:   Generate  $\mathcal{M}'$  via intra-population crossover in  $\mathcal{P}$ .  $\triangleright$  Eq. (6)
4:   Mutate  $\mathcal{M}'$ .  $\triangleright$  Eq. (5)
5: end for
6: while not converged do
7:   for each  $\mathcal{P}$  do
8:     Optimize  $\mathcal{M}'$  with  $\alpha', \beta'$ .  $\triangleright$  Eq. (4)
9:     if  $\text{mod}(t, \tau) = 0$  then
10:      Select the worst  $\mathcal{M}$ .  $\triangleright$  Eq. (8)
11:      Replace  $\mathcal{M}$  in  $\mathcal{P}$  with  $\mathcal{M}'$ .
12:      if  $\text{mod}(t, ep \times \tau) \neq 0$  then
13:        Generate  $\mathcal{M}'$  via intra-population crossover.
14:        Mutate  $\mathcal{M}'$ .  $\triangleright$  Eq. (5)
15:      end if
16:    end if
17:   end for
18:   if  $\text{mod}(t, ep \times \tau) = 0$  then
19:     Choose  $(\mathcal{P}_A, \mathcal{P}_B)$  either by task or lake type.
20:     Generate  $(\mathcal{M}'_A, \mathcal{M}'_B)$  via inter-population crossover between  $\mathcal{P}_A, \mathcal{P}_B$ .  $\triangleright$  Eq. (7)
21:     for each  $\mathcal{P}$  not in  $(\mathcal{P}_A, \mathcal{P}_B)$  do
22:       Generate  $\mathcal{M}'$  via intra-population crossover.
23:     end for
24:     for each  $\mathcal{P}$  do
25:       Mutate  $\mathcal{M}'$ .  $\triangleright$  Eq. (5)
26:     end for
27:   end if
28: end while
29: return the set of best models, one from each population  $\mathcal{P}$ :
    $\mathcal{M} = \arg \min_{\mathcal{M}_v \in \mathcal{P}} L(\mathcal{M}_v)$ .

```

where \hat{y}_t denotes the predicted DO concentration, y_t is the observed DO concentration, \tilde{y}_t is the simulated DO concentration, $\mathbb{I}(x)$ is an indicator function that equals 1 if x is observed (true) and 0 otherwise (false), and ρ is the tradeoff parameter assigned to blending observed and simulated labels.

4 EXPERIMENTAL EVALUATION

We conduct extensive experiments across a variety of north temperate lakes in the Midwest, USA, to investigate the research questions:

- **RQ1.** How does the effectiveness of the NGCE strategy compare to other baseline models?
- **RQ2.** What is the performance of the NGCE strategy in time-series analysis of DO concentrations?
- **RQ3.** How do feature interactions vary across lake types and tasks, and how do these interactions evolve over multiple years?
- **RQ4.** How significant and effective are the feature interactions selected by the NGCE strategy?

Table 1: Comparative performance of DO concentration (g/m^3) prediction in terms of root mean square error (RMSE) across different lake types and tasks. The mean and standard deviation (displayed in grey) of RMSE are calculated from ten runs.

Algo. Name	Small lakes		Medium lakes		Large lakes		Extra-large lakes	
	Epi.	Hyp.	Epi.	Hyp.	Epi.	Hyp.	Epi.	Hyp.
Sim DO conc.	1.943 (0.000)	2.212 (0.000)	1.940 (0.000)	2.217 (0.000)	2.620 (0.000)	2.937 (0.000)	1.536 (0.000)	2.772 (0.000)
LSTM	1.802 (0.079)	1.973 (0.064)	1.744 (0.092)	2.001 (0.081)	2.298 (0.088)	2.630 (0.043)	1.479 (0.068)	2.594 (0.056)
EA-LSTM	1.716 (0.047)	1.783 (0.098)	1.676 (0.084)	1.546 (0.054)	2.111 (0.045)	2.629 (0.043)	1.478 (0.039)	2.278 (0.062)
KGSSL	1.793 (0.044)	1.467 (0.057)	1.557 (0.062)	1.632 (0.094)	2.064 (0.103)	2.730 (0.060)	1.294 (0.047)	2.425 (0.075)
AutoInt	1.510 (0.080)	1.406 (0.097)	1.516 (0.088)	1.626 (0.094)	1.716 (0.072)	1.924 (0.078)	1.112 (0.081)	1.847 (0.085)
AutoGroup	1.473 (0.078)	1.509 (0.080)	1.364 (0.059)	1.875 (0.072)	1.384 (0.075)	1.600 (0.068)	0.937 (0.085)	1.953 (0.076)
AutoFeature	1.382 (0.063)	1.768 (0.089)	1.422 (0.070)	1.467 (0.081)	1.405 (0.084)	1.465 (0.082)	1.178 (0.078)	1.976 (0.093)
NGCE	1.076 (0.146)	1.316 (0.161)	1.060 (0.137)	1.288 (0.159)	0.988 (0.169)	1.243 (0.156)	0.918 (0.171)	1.415 (0.215)

4.1 Experimental Settings

4.1.1 Dataset. We evaluate the proposed NGCE strategy for predicting DO concentration using a dataset from the North Temperate Lakes Long-Term Ecological Research program¹ [37], which documents over 41 years of ecological observations from 375 lakes in the Midwest, USA, starting in 1979. This dataset has grown to include around 5.58 million daily records, each characterized by 39 fields of phenological features, including morphometric, flux data, weather conditions, trophic states, and land use details. Observed DO data were sourced from the Water Quality Portal (WQP). Lake residence time was taken from the HydroLAKES dataset². Trophic state probabilities (eutrophic, oligotrophic, dystrophic) were from a recently published dataset [40]. Land use proportions of each lake’s watershed were taken from the National Land Cover Database (NLCD). An account of these features is available in the **Appendix**. Of these, 36,920 records include measured DO concentrations for both the upper epilimnion and the lower hypolimnion layers. We split the dataset as follows: data collected until 2017 are for training the models for larger and extra-large lakes, with 2018 for validation, and 2019 for testing. For small and medium lakes, where DO observations in 2019 are comparatively sparse, we resort to data up until 2016 for training, 2017 for validation, and 2018 for testing.

4.1.2 Baselines. We compare to a set of baselines in our experiment: *Sim DO Conc.*: This baseline is the metabolic process-based model used in our first stage, leveraging minimal observed labels to generate simulations that can significantly augment the data for other baselines. *LSTM*: As adopted in our model functioning stage, LSTM incorporates simulated labels for weighted imputation and backward gradient adjustments, a necessity for convergence given the scarcity of observed labels. *EA-LSTM & KGSSL* [10, 28]: These time series prediction models, which assimilate hydrological behavior and physical processes, respectively, are regarded as cutting-edge within hydrological and ecological domains. LSTM and EA-LSTM, along with KGSSL, adopt individual features for input without feature interaction modeling. *AutoInt, AutoGroup, & AutoFeature* [26, 32, 52]: Emblematic of state-of-the-art feature interaction modeling, these methods have demonstrated their utility and versatility through extensive commercial deployment, showcasing their capacity to model complex feature combinations.

¹<https://lter.limnology.wisc.edu/>

²<https://www.hydrosheds.org/pages/hydrolakes>

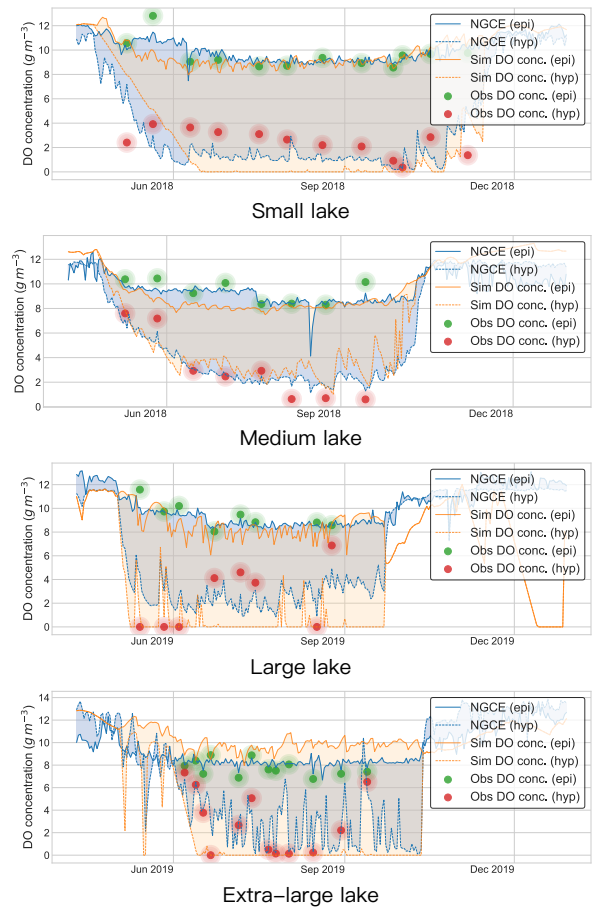


Figure 2: Time-series analysis of DO concentrations: a comparison of predicted (NGCE), simulated, and observed values.

4.1.3 Implementation Details. To implement NGCE, we set feature embedding size $|f_t| = 15$. We use RDA optimizer [6, 62] to discriminate the relevant and irrelevant feature interactions, with the learning rate $\gamma = 10^{-3}$, adjustable hyperparameters $c = 0.5$, $\mu = 0.8$. We set the population size as $n = 4$. We set the mutation mechanism as the mutation threshold $\lambda = 0.2$, the mutation probability $\sigma = 0.5$, and the mutation step size $\tau = 10$. We set the inter-population crossover step size $ep = 10$, and the tradeoff parameter $\rho = 0.1$.

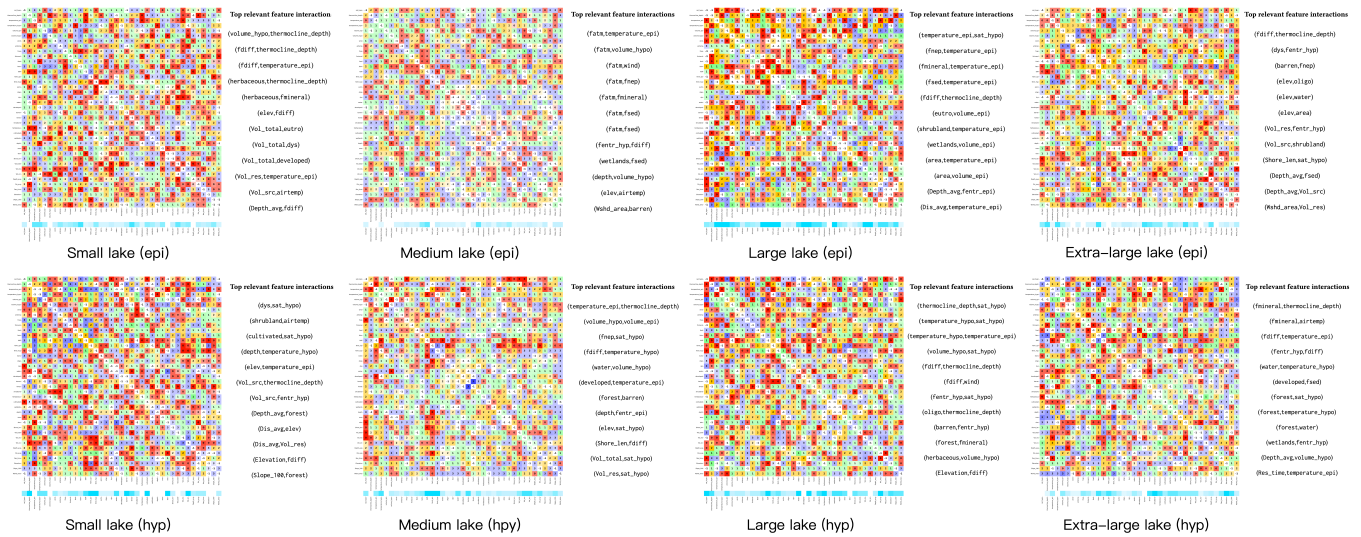


Figure 3: Visualization of gene maps highlighting top relevant feature interactions across different lake types and tasks.

4.2 Experimental Results

4.2.1 Performance comparison (RQ1). Table 1 presents a comparative analysis of the NGCE strategy against various baselines, utilizing root mean square error (RMSE) across diverse lake types and tasks, with both mean and standard deviation calculated over five runs. From the results, we have the following key observations:

First, machine learning models universally outperform simulations alone, underscoring the value of integrating observed labels with simulated labels for enhanced prediction accuracy. Second, EA-LSTM and KGSSL surpass LSTM in performance, evidencing the advantage of incorporating hydrological behaviors and physical processes into models, particularly when faced with a scarcity of labels. Third, AutoInt, AutoGroup, and AutoFeature demonstrate the predictive power of feature interactions, offering significant improvements over models that rely solely on individual feature inputs. Lastly, NGCE emerges as the superior model across all baselines, attributing its success to the adaptive modeling of interactions through evolutionary operation selection. Unlike methods that indiscriminately consider all features and interactions, NGCE discerns their relevance to specific lake types and tasks, thereby amplifying the impact of relevant features and interactions while diminishing or altering those of lesser relevance. However, NGCE’s performance variability, as evidenced by the relatively wide standard deviation across trials, points to algorithmic instability—a consequence of its meta-heuristic nature dependent on stochastic processes.

4.2.2 Time-series analysis (RQ2). Figure 2 offers a time-series comparison of predicted (NGCE), simulated, and observed DO concentrations, with a specific emphasis on the summer season of the testing period. The analysis reveals that NGCE predictions not only align closely with observed values but also demonstrate sensitivity to subtle features and interactions, enhancing their accuracy. While simulated DO concentrations also generally exhibit a clear trend, there are instances of slight deviation from observed data. Encouragingly, both predicted and simulated values largely mirror observed trends, highlighting the efficacy and significance of our NGCE strategy in advancing research in this domain.

4.2.3 Visualization of gene maps (RQ3). The model populations accommodate different lake types and tasks, leading to a rich diversity in model traits. These traits influence their survival and fitness rates, mirroring the selection process for operations and feature interactions. To demonstrate the model’s evolutionary process and how feature interactions adapt across different lake types and tasks, we visualize the model’s **gene maps**. Adopting an encoding where $\oplus = 0, \otimes = 1, \boxplus = 2, \boxtimes = 3$, we can diagnose the model’s fitness as a symmetric matrix. Distinct colors are allocated to each operation, creating a vibrant gene map where each gene symbolizes an interaction; like red "0", green "1", yellow "2", and blue "3". For example, a green "1" within the "depth × area" block signifies that the element-wise product \otimes is identified as the optimal operation for "depth" to interact with "area". The intensity of the colors on the gene map is directly correlated with the relevance of the interactions, with darker hues denoting higher relevance and lighter ones suggesting lesser importance. Individual features are also visually encoded as single-hued bars. Interactions deemed irrelevant, with their relevance parameters reduced to 0, are excluded, leaving their corresponding genes depicted in white "–1".

Figure 3 presents gene maps based on end-of-training data, showcasing highlight relevant feature interactions for DO concentration prediction, offering insight into their relevance across different lake sizes and stratification dynamics. In larger lakes, the DO dynamics are predominantly influenced by sediment oxygen demand and atmospheric exchange, reflecting their extensive water volumes. Conversely, smaller lakes exhibit DO concentrations that are notably impacted by local land use and meteorological factors due to their shallower depths and greater vulnerability to changes in their external watershed environments. Across the board, temperature-related interactions are significant, affecting DO solubility and the lake’s biological processes. Additionally, wind speed and atmospheric exchange flux stand out as key drivers of surface gas exchange influencing epilimnion, while the trophic state markers provide indicators of possible oxygen production in the epilimnion and eventual hypolimnetic depletion due to the formation of algal

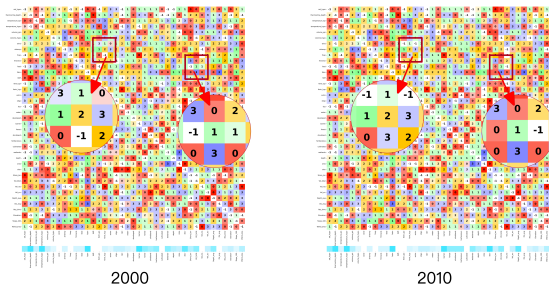


Figure 4: Gene maps that evolved over ten years.

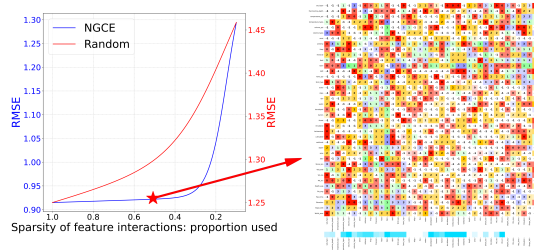


Figure 5: Impact of increasing feature interaction sparsity.

blooms. These findings suggest that diverse ecological factors interplay differently across lake environments, necessitating adaptable prediction models that can cater to these variances.

Figure 4 presents a comparison of gene maps for extra-large lakes across a decade, from 2000 to 2010. The enduring patterns of feature interactions hint at consistent ecological processes, while deviations in their relevance suggest adaptation to environmental shifts and human activities. Changes in the importance of certain interactions may stem from better land management or climate variations affecting lake stratification. Meanwhile, the emergence of new significant interactions could be a reaction to changes in lake usage or watershed practices. These temporal dynamics highlight the importance of adaptable models like NGCE, which can recalibrate the significance of feature interactions to align with the changing lake environments over time.

4.2.4 Impact of selected feature interactions (RQ4). As depicted in Figure 5, we evaluate the impact of feature interactions identified by the NGCE strategy. By adjusting the RDA optimizer’s parameters, we consistently choose a sparser set of feature interactions, accepting a trade-off in accuracy, illustrated by the blue trend line for NGCE. Simultaneously, a random strategy is applied for comparative purposes, where operations for feature interactions are allocated at random, and some interactions are arbitrarily removed as sparsity intensifies, as depicted by the red trend line. The gene map showcased at a feature interaction sparsity level around 0.5 offers insight into the model’s structure under reduced complexity. This experiment highlights NGCE’s superior performance even as many feature interactions are discarded, emphasizing its precision in identifying relevant interactions under task guidance. Conversely, the random approach shows a quicker performance drop due to the loss of important interactions. When feature interactions become exceedingly sparse, both methodologies suffer in performance, indicating that a limited set of feature interactions fails to significantly contribute to the model’s predictive capabilities. In such scenarios, it is predominantly the individual features that influence the model’s performance.

5 RELATED WORK

Aquatic ecosystem models (AEMs) have been pivotal in the aquatic ecosystem science domain, helping us understand the complex interactions within ecosystems [20]. These models blend hydrodynamics, water quality, and ecosystem processes, employing various methodologies such as DYRESM [13], GLM [17], MyLake [48], GOTM [5], LAKE2.0 [55], and Simstrat [12]. More advanced vertical one-dimensional AEMs including GLM-AED [17], WET [41], and PCLake [21] further enhance modeling capabilities.

Despite their comprehensive nature, AEMs encounter limitations due to their complexity, computational intensity, and equifinality issues, constraining their flexibility and wider applicability [3, 36]. Simpler diel metabolism models, while insightful for short-term DO fluctuations, often overlook long-term ecosystem predictions due to missing hydrodynamic factors [1, 7, 11, 19, 47, 54]. Bridging these gaps, integrating physics-based models with machine learning offers groundbreaking potential [9, 15, 23, 31, 35, 43, 45, 58, 59], especially by using simulated data from physics-based models to enhance ML training in light of limited observed data [8, 14, 44].

Predicting DO concentrations in aquatic environments highlights the need to carefully choose and examine phenological features and their interactions [22, 42, 49, 53, 61]. This emphasizes the value of assessing feature interactions to enhance prediction accuracy, as supported by research emphasizing embedded methods for feature interaction selection [63, 65]. Traditionally, interaction modeling employed methodologies like factorization machines (FM) [46] and field-aware FM (FFM) [24], which faced limitations in representation capability. However, a uniform application of predefined operations across all feature interactions, often under expert guidance, might not always align with the specific demands of tasks or data, potentially introducing noise and complicating the training process [33, 64]. Herein, adaptive learning, utilizing nature-inspired meta-heuristic algorithms or gradient-based AutoML, presents a powerful solution for complex search challenges in machine learning [2, 25, 66]. Feature selection methods in AutoML, especially within embedded frameworks that combine feature selection and classifier training, face difficulties in evaluating model fitness accurately [26, 32, 52, 57, 63]. Our strategy aims to overcome these challenges by refining feature interaction selection with evolutionary strategies, thereby improving model adaptability for the intricate task of aquatic ecosystem management.

6 CONCLUSION

This paper presents the *Nature-Guided Cognitive Evolution (NGCE)* strategy, a novel approach blending adaptive learning with natural processes for predicting dissolved oxygen (DO) concentrations in north temperate lakes. NGCE analyzes intricate phenological patterns and utilizes evolutionary learning for feature interaction selection, mirroring the adaptability inherent in natural organisms. It employs multi-population models customized for varied lake types and tasks, reflecting the diverse survival strategies of species across various habitats. Evaluated on a variety of north temperate lakes in the Midwest, USA, NGCE not only demonstrates accurate DO concentration predictions with limited observed data but also reveals sophisticated phenological patterns, highlighting its utility for environmental science and lake management.

REFERENCES

- [1] Alison P Appling, Robert O Hall Jr, Charles B Yackulic, and Maite Arroita. 2018. Overcoming equifinality: Leveraging long time series for stream metabolism estimation. *Journal of Geophysical Research: Biogeosciences* 123, 2 (2018), 624–645.
- [2] Thomas Back. 1996. *Evolutionary algorithms in theory and practice: evolution strategies, evolutionary programming, genetic algorithms*. Oxford University Press.
- [3] Keith Beven. 2006. A manifesto for the equifinality thesis. *Journal of hydrology* 320, 1–2 (2006), 18–36.
- [4] Edward Asahel Birge. 1906. Gases dissolved in the waters of Wisconsin lakes. *Transactions of the American Fisheries Society* 35, 1 (1906), 143–163.
- [5] Hans Burchard, Karsten Bolding, and Manuel R Villarreal. 1999. *GOTM, a general ocean turbulence model: theory, implementation and test cases*. Space Applications Institute.
- [6] Shih-Kang Chao and Guang Cheng. 2019. A generalization of regularized dual averaging and its dynamics. *arXiv preprint arXiv:1909.10072* (2019).
- [7] James J Coloso, Jonathan J Cole, Paul C Hanson, and Michael L Pace. 2008. Depth-integrated, continuous estimates of metabolism in a clear-water lake. *Canadian Journal of Fisheries and Aquatic Sciences* 65, 4 (2008), 712–722.
- [8] Felix Finkeldey, Julia Volke, Jan-Christoph Zarges, Hans-Peter Heim, and Petra Wiederkehr. 2020. Learning quality characteristics for plastic injection molding processes using a combination of simulated and measured data. *Journal of Manufacturing Processes* 60 (2020), 134–143.
- [9] Gohar Ghazaryan, Sergii Skakun, Simon König, Ehsan Eyshi Rezaei, Stefan Siebert, and Olena Dubovyk. 2020. Crop yield estimation using multi-source satellite image series and deep learning. In *IGARSS 2020-2020 IEEE International Geoscience and Remote Sensing Symposium*. IEEE, 5163–5166.
- [10] Rahul Ghosh, Arvind Renganathan, Kshitij Tayal, Xiang Li, Ankush Khandelwal, Xiaowei Jia, Christopher Duffy, John Nieber, and Vipin Kumar. 2022. Robust inverse framework using knowledge-guided self-supervised learning: An application to hydrology. In *Proceedings of the 28th ACM SIGKDD Conference on Knowledge Discovery and Data Mining*. 465–474.
- [11] Darren P Giling, Peter A Staehr, Hans Peter Grossart, Mikkel René Andersen, Bertram Boehrer, Carmelo Escot, Fatih Evrendilek, Luis Gómez-Gener, Mark Honti, Ian D Jones, et al. 2017. Delving deeper: Metabolic processes in the metalimnion of stratified lakes. *Limnology and Oceanography* 62, 3 (2017), 1288–1306.
- [12] G-H Goudsmit, Hans Burchard, Frank Peeters, and Alfred Wüest. 2002. Application of k-epsilon turbulence models to enclosed basins: the role of internal seiches. *Journal of Geophysical Research: Oceans* 107, C12 (2002), 23–1.
- [13] David P Hamilton and S Geoffrey Schladow. 1997. Prediction of water quality in lakes and reservoirs. Part I—Model description. *Ecological modelling* 96, 1–3 (1997), 91–110.
- [14] Herim Han and Sunghwan Choi. 2021. Transfer Learning from Simulation to Experimental Data: NMR Chemical Shift Predictions. *The Journal of Physical Chemistry Letters* 12, 14 (2021), 3662–3668.
- [15] Paul C Hanson, Aviah B Stillman, Xiaowei Jia, Anuj Karpatne, Hilary A Dugan, Cayelan C Carey, Joseph Stachelek, Nicole K Ward, Yu Zhang, and Jordan S Read. [n.d.]. Predicting lake surface water phosphorus dynamics using process-guided machine learning. 430 (n.d.), 109136.
- [16] Jun He and Xin Yao. 2002. From an individual to a population: An analysis of the first hitting time of population-based evolutionary algorithms. *IEEE Transactions on Evolutionary Computation* 6, 5 (2002), 495–511.
- [17] Matthew R Hipsey, Louise C Bruce, Casper Boon, Brendan Busch, Cayelan C Carey, David P Hamilton, Paul C Hanson, Jordan S Read, Eduardo de Sousa, Michael Weber, et al. 2019. A General Lake Model (GLM 3.0) for linking with high-frequency sensor data from the Global Lake Ecological Observatory Network (GLEON). *Geoscientific Model Development* 12, 1 (2019), 473–523.
- [18] Sepp Hochreiter and Jürgen Schmidhuber. 1997. Long short-term memory. *Neural computation* 9, 8 (1997), 1735–1780.
- [19] Gordon W Holtgrieve, Daniel E Schindler, Trevor A Branch, and Z Teresa A'mar. 2010. Simultaneous quantification of aquatic ecosystem metabolism and reaeration using a Bayesian statistical model of oxygen dynamics. *Limnology and Oceanography* 55, 3 (2010), 1047–1063.
- [20] Annette BG Janssen, George B Arhonditsis, Arthur Beusen, Karsten Bolding, Louise Bruce, Jorn Bruggeman, Raoul-Marie Couture, Andrea S Downing, J Alex Elliott, Marieke A Frassl, et al. 2015. Exploring, exploiting and evolving diversity of aquatic ecosystem models: a community perspective. *Aquatic Ecology* 49 (2015), 513–548.
- [21] Annette BG Janssen, Sven Teurlinckx, Arthur HW Beusen, Mark AJ Huijbregts, Jasmijn Rost, Aafke M Schipper, Laura MS Seelen, Wolf M Mooij, and Jan H Janse. 2019. PCLake+: A process-based ecological model to assess the trophic state of stratified and non-stratified freshwater lakes worldwide. *Ecological modelling* 396 (2019), 23–32.
- [22] Jean-Philippe Jenny, Alexandre Normandeau, Pierre Francus, Zofia Ecaterina Taranu, Irene Gregory-Eaves, François Lapointe, Josue Jautzy, Antti EK Ojala, Jean-Marcel Dorioz, Arndt Schimmelmann, et al. 2016. Urban point sources of nutrients were the leading cause for the historical spread of hypoxia across European lakes. *Proceedings of the National Academy of Sciences* 113, 45 (2016), 12655–12660.
- [23] Xiaowei Jia, Ankush Khandelwal, David J Mulla, Philip G Pardey, and Vipin Kumar. 2019. Bringing automated, remote-sensed, machine learning methods to monitoring crop landscapes at scale. *Agricultural Economics* 50 (2019), 41–50.
- [24] Yuchin Juan, Yong Zhuang, Wei-Sheng Chin, and Chih-Jen Lin. 2016. Field-aware factorization machines for CTR prediction. In *Proceedings of the 10th ACM Conference on Recommender Systems (RecSys)*. 43–50.
- [25] Chia-Feng Juang, Ching-Yu Chou, and Chin-Teng Lin. 2022. Navigation of a fuzzy-controlled wheeled robot through the combination of expert knowledge and data-driven multiobjective evolutionary learning. *IEEE Transactions on Cybernetics* 52, 8 (2022), 7388–7401.
- [26] Farhan Khawar, Xu Hang, Ruiming Tang, Bin Liu, Zhenguo Li, and Xiuqiang He. 2020. Autofeature: Searching for feature interactions and their architectures for click-through rate prediction. In *ACM International Conference on Information and Knowledge Management (CIKM)*. 625–634.
- [27] Diederik P Kingma and Jimmy Ba. 2014. Adam: A method for stochastic optimization. *arXiv preprint arXiv:1412.6980* (2014).
- [28] Frederik Kratzert, Daniel Klotz, Guy Shalev, Günter Klambauer, Sepp Hochreiter, and Grey Nearing. 2019. Towards learning universal, regional, and local hydrological behaviors via machine learning applied to large-sample datasets. *Hydrology and Earth System Sciences* 23, 12 (2019), 5089–5110.
- [29] Robert Ladwig, Alison P Appling, Austin Delany, Hilary A Dugan, Qiantong Gao, Noah Lottig, Jemma Stachelek, and Paul C Hanson. 2022. Long-term change in metabolism phenology in north temperate lakes. *Limnology and Oceanography* 67, 7 (2022), 1502–1521.
- [30] Yann LeCun, Yoshua Bengio, and Geoffrey Hinton. 2015. Deep learning. *nature* 521, 7553 (2015), 436–444.
- [31] LIU Licheng, Wang Zhou, Zhenong Jin, Jinyun Tang, Xiaowei Jia, Chongya Jiang, Kaiyu Guan, Bin Peng, Shaoming Xu, Yufeng Yang, et al. 2021. Estimating the Autotrophic and Heterotrophic Respiration in the US Crop Fields using Knowledge Guided Machine Learning. In *AGU Fall Meeting 2021*. AGU.
- [32] Bin Liu, Niannan Xue, Huifeng Guo, Ruiming Tang, Stefanos Zafeiriou, Xiuqiang He, and Zhenguo Li. 2020. AutoGroup: Automatic feature grouping for modelling explicit high-order feature interactions in CTR prediction. In *Proceedings of the 43rd international ACM SIGIR conference on Research and Development in Information Retrieval (SIGIR)*. 199–208.
- [33] Bin Liu, Chenxu Zhu, Guilin Li, Weinan Zhang, et al. 2020. Autofis: Automatic feature interaction selection in factorization models for click-through rate prediction. In *Proceedings of the 26th ACM SIGKDD International Conference on Knowledge Discovery & Data Mining (KDD)*. 2636–2645.
- [34] Hanxiao Liu, Karen Simonyan, and Yiming Yang. 2019. DARTS: Differentiable architecture search. In *International Conference on Learning Representations*.
- [35] Licheng Liu, Shaoming Xu, Jinyun Tang, Kaiyu Guan, Timothy J Griffis, Matthew D Erickson, Alexander L Frie, Xiaowei Jia, Taegon Kim, Lee T Miller, et al. 2022. KGML-ag: a modeling framework of knowledge-guided machine learning to simulate agroecosystems: a case study of estimating N₂O emission using data from mesocosm experiments. *Geoscientific Model Development* 15, 7 (2022), 2839–2858.
- [36] Liancong Luo, David Hamilton, Jia Lan, Chris McBride, and Dennis Trolle. 2018. Autocalibration of a one-dimensional hydrodynamic-ecological model (DYRESM 4.0-CAEDYM 3.1) using a Monte Carlo approach: simulations of hypoxic events in a polymictic lake. *Geoscientific Model Development* 11, 3 (2018), 903–913.
- [37] John J Magnuson, Timothy K Kratz, and Barbara J Benson. 2006. *Long-term dynamics of lakes in the landscape: long-term ecological research on north temperate lakes*. Long-Term Ecological Research.
- [38] Mikko I Malinen and Pasi Fränti. 2014. Balanced k-means for clustering. In *Structural, Syntactic, and Statistical Pattern Recognition: Joint IAPR International Workshop, S+ SSPR 2014, Joensuu, Finland, August 20–22, 2014. Proceedings*. Springer, 32–41.
- [39] Rammohan Mallipeddi and Ponnuthurai N Suganthan. 2008. Empirical study on the effect of population size on differential evolution algorithm. In *2008 IEEE Congress on Evolutionary Computation*. IEEE, 3663–3670.
- [40] Michael F Meyer, Simon N Topp, Tyler V King, Robert Ladwig, Rachel M Pilla, Hilary A Dugan, Jack R Eggleston, Stephanie E Hampton, Dina M Leech, Isabella A Oleksy, et al. 2024. National-scale remotely sensed lake trophic state from 1984 through 2020. *Scientific Data* 11, 1 (2024), 77.
- [41] Anders Nielsen, Karsten Bolding, Fenjuan Hu, and Dennis Trolle. 2017. An open source QGIS-based workflow for model application and experimentation with aquatic ecosystems. *Environmental Modelling & Software* 95 (2017), 358–364.
- [42] Joseph S Phillips. 2020. Time-varying responses of lake metabolism to light and temperature. *Limnology and Oceanography* 65, 3 (2020), 652–666.
- [43] Farshid Rahmani, Kathryn Lawson, Wenyu Ouyang, Alison Appling, Samantha Oliver, and Chaopeng Shen. 2021. Exploring the exceptional performance of a deep learning stream temperature model and the value of streamflow data. *Environmental Research Letters* 16, 2 (2021), 024025.

- [44] Stephan Rasp and Nils Thuerey. 2021. Data-driven medium-range weather prediction with a resnet pretrained on climate simulations: A new model for weatherbench. *Journal of Advances in Modeling Earth Systems* 13, 2 (2021), e2020MS002405.
- [45] Jordan S Read, Xiaowei Jia, Jared Willard, Alison P Appling, Jacob A Zwart, Samantha K Oliver, Anuj Karpatne, Gretchen JA Hansen, Paul C Hanson, William Watkins, et al. 2019. Process-guided deep learning predictions of lake water temperature. *Water Resources Research* 55, 11 (2019), 9173–9190.
- [46] Steffen Rendle. 2010. Factorization machines. In *2010 IEEE International Conference on Data Mining (ICDM)*. IEEE, 995–1000.
- [47] Steven Sadro, John M Melack, and Sally MacIntyre. 2011. Depth-integrated estimates of ecosystem metabolism in a high-elevation lake (Emerald Lake, Sierra Nevada, California). *Limnology and oceanography* 56, 5 (2011), 1764–1780.
- [48] Tuomo M Saloranta and Tom Andersen. 2007. MyLake—A multi-year lake simulation model code suitable for uncertainty and sensitivity analysis simulations. *Ecological modelling* 207, 1 (2007), 45–60.
- [49] Christopher T Solomon, Denise A Bruesewitz, David C Richardson, Kevin C Rose, Matthew C Van de Bogert, Paul C Hanson, Timothy K Kratz, Bret Larget, Rita Adrian, Brenda Leroux Babin, et al. 2013. Ecosystem respiration: drivers of daily variability and background respiration in lakes around the globe. *Limnology and Oceanography* 58, 3 (2013), 849–866.
- [50] Ulrich Sommer, Rita Adrian, Lisette De Senerpont Domis, James J Elser, Ursula Gaedke, Bas Ibelings, Erik Jeppesen, Miquel Lürling, Juan Carlos Molinero, Wolf M Mooij, et al. 2012. Beyond the Plankton Ecology Group (PEG) model: mechanisms driving plankton succession. *Annual review of ecology, evolution, and systematics* 43 (2012), 429–448.
- [51] Qingquan Song, Dehua Cheng, Hanning Zhou, Jiyan Yang, Yuandong Tian, and Xia Hu. 2020. Towards automated neural interaction discovery for click-through rate prediction. In *Proceedings of the 26th ACM SIGKDD International Conference on Knowledge Discovery & Data Mining (KDD)*. 945–955.
- [52] Weiping Song, Chence Shi, Zhiping Xiao, Zhijian Duan, Yewen Xu, Ming Zhang, and Jian Tang. 2019. AutoInt: Automatic feature interaction learning via self-attentive neural networks. In *ACM International Conference on Information and Knowledge Management (CIKM)*. 1161–1170.
- [53] Peter A Staehr, Darren Bade, Matthew C Van de Bogert, Gregory R Koch, Craig Williamson, Paul Hanson, Jonathan J Cole, and Tim Kratz. 2010. Lake metabolism and the diel oxygen technique: state of the science. *Limnology and Oceanography: Methods* 8, 11 (2010), 628–644.
- [54] Peter A Staehr, Jeremy M Testa, W Michael Kemp, Jon J Cole, Kaj Sand-Jensen, and Stephen V Smith. 2012. The metabolism of aquatic ecosystems: history, applications, and future challenges. *Aquatic Sciences* 74 (2012), 15–29.
- [55] Victor Stepanenko, Ivan Mammarella, Anne Ojala, Heli Miettinen, Vasily Lykosov, and Timo Vesala. 2016. LAKE 2.0: a model for temperature, methane, carbon dioxide and oxygen dynamics in lakes. *Geoscientific Model Development* 9, 5 (2016), 1977–2006.
- [56] Ke Tang, Peng Yang, and Xin Yao. 2016. Negatively correlated search. *IEEE Journal on Selected Areas in Communications* 34, 3 (2016), 542–550.
- [57] Akbar Telikani, Amirhessam Tahmassebi, et al. 2021. Evolutionary machine learning: A survey. *Comput. Surveys* 54, 8 (2021), 1–35.
- [58] Thomas Van Klompenburg, Ayalew Kassahun, and Gagayatal Catal. 2020. Crop yield prediction using machine learning: A systematic literature review. *Computers and Electronics in Agriculture* 177 (2020), 105709.
- [59] Jared D Willard, Jordan S Read, Alison P Appling, Samantha K Oliver, Xiaowei Jia, and Vipin Kumar. 2021. Predicting Water Temperature Dynamics of Unmonitored Lakes With Meta-Transfer Learning. *Water Resources Research* 57, 7 (2021), e2021WR029579.
- [60] P Chris Wilson. 2010. Water Quality Notes: Dissolved Oxygen: SL313/SS525, 1/2010. *EDIS* 2010, 2 (2010).
- [61] R Iestyn Woolway, Sapna Sharma, Gesa A Weyhenmeyer, Andrey Debolskiy, Malgorzata Golub, Daniel Mercado-Bettin, Marjorie Perroud, Victor Stepanenko, Zeli Tan, Luke Grant, et al. 2021. Phenological shifts in lake stratification under climate change. *Nature communications* 12, 1 (2021), 2318.
- [62] Lin Xiao. 2009. Dual averaging method for regularized stochastic learning and online optimization. *Advances in Neural Information Processing Systems* 22 (2009).
- [63] Bing Xue, Mengjie Zhang, Will N Browne, and Xin Yao. 2015. A survey on evolutionary computation approaches to feature selection. *IEEE Transactions on Evolutionary Computation* 20, 4 (2015), 606–626.
- [64] Runlong Yu, Xiang Xu, Yuyang Ye, Qi Liu, and Enhong Chen. 2023. Cognitive Evolutionary Search to Select Feature Interactions for Click-Through Rate Prediction. In *Proceedings of the 29th ACM SIGKDD Conference on Knowledge Discovery and Data Mining*. 3151–3161.
- [65] Runlong Yu, Yuyang Ye, Qi Liu, Zihan Wang, Chunfeng Yang, Yucheng Hu, and Enhong Chen. 2021. Xcrossnet: Feature structure-oriented learning for click-through rate prediction. In *Advances in Knowledge Discovery and Data Mining: 25th Pacific-Asia Conference (PAKDD)*. Springer, 436–447.
- [66] Zhi-Hua Zhou, Yang Yu, and Chao Qian. 2019. *Evolutionary learning: Advances in theories and algorithms*. Springer.

A APPENDIX

Table 2: Features for DO Concentration Prediction

Feature Group	Feature Descriptions
Morphometric & Geographic	depth: Derived maximum lake depth
	area: Derived maximum lake surface area
	elev: Derived lake elevation
	Shore_len: Shore length
	Vol_total: Lake volume
	Vol_res: Lake volume residual
	Vol_src: Lake volume supplement
	Depth_avg: Average lake depth
	Dis_avg: Average inflow discharge
	Res_time: Lake residence time
Elevation: Alternative lake elevation	
Slope_100: Lake slope information	
Wshd_area: Watershed area	
Mass Fluxes	fnep: Net ecosystem production flux
	fmineral: Mineralisation flux
	fsed: Net sedimentation flux
	fatm: Atmospheric exchange flux.
	fdiff: Diffusion flux
fentr_epi: Entrainment flux in the epilimnion	
fentr_hyp: Entrainment flux in the hypolimnion	
Weather Conditions	wind: Derived wind speed
	airtemp: Derived air temperature
Trophic State	eutro: Derived classification for eutrophic state
	oligo: Derived classification for oligotrophic state
	dys: Derived classification for dystrophic state
Watershed Land Use	water: Derived classification proportion for water land use
	developed: Derived classification proportion for developed land use
	barren: Derived classification proportion for barren land use
	forest: Classification proportion for forest land use
	shrubland: Derived classification proportion for shrubland land use
	herbaceous: Derived classification proportion for herbaceous land use
	cultivated: Derived classification proportion for cultivated land use
	wetlands: Derived classification proportion for wetlands land use
	Stratification
thermocline_dept: Thermocline depth	
temperature_epi: Epilimnion water temperature	
temperature_hypo: Hypolimnion water temperature	
volume_epi: Epilimnion volume	
volume_hypo: Hypolimnion volume	